PAPER • OPEN ACCESS

Developing printable thermoelectric materials based on graphene nanoplatelet/ethyl cellulose nanocomposites

View the article online for updates and enhancements.

IOP ebooks™

Bringing together innovative digital publishing with leading authors from the global scientific community.

Start exploring the collection−download the first chapter of every title for free.

Materials Research Express

Developing printable thermoelectric materials based on graphene nanoplatelet/ethyl cellulose nanocomposites

Saeed Mardi ⬝ , Marco Risi Ambrogioni and Andrea Reale

Department of Electronic Engineering, CHOSE—Centre for Hybrid and Organic Solar Energy, University of Rome Tor Vergata, via del Politecnico 1, 00133 Rome, Italy

E-mail: reale@uniroma2.it

Abstract

Thermoelectric (TE) materials have drawn a lot of attention as a promising technology to harvest waste heat and convert it into electrical energy. However, the toxicity and expense of inorganic TE materials along with high-temperature fabrication processes have limited their application. Additionally, the reduction of raw material resources, such as metals and petroleum is another limiting factor. Hence, developing low-cost, stable, and easily-created TE materials from renewable resources is attracting more and more interest for a wide range of applications including the internet of things and self-powered sensors. Herein, an efficacious processing strategy to fabricate printable TE materials has been developed with Ethyl cellulose (EC), a non-conducting polymer, as the polymer matrix and with Graphene nanoplatelets (GNPs) as fillers. EC, one of the cellulose's derivatives, has been widely used as a binder in the printing pastes. The conductive pastes with different filler contents have been fabricated. The weight ratio of GNPs and EC were ranged from 0.2 to 0.7. These conductive pastes have been deposited by blade coating on glass substrates. The electrical conductivity of the composites has increased polynomially as the filler content increased, whereas the Seebeck coefficient did not change significantly with the increased electrical conductivity. The highest electrical conductivity at room temperature (355.4 S m^{-1}) was obtained for the ratio of 0.7. This ratio also had the maximum power factor value. Moreover, a 3D structure form (cylindrical pellet) from the highest conductive paste was also fabricated. The proposed technique demonstrates an industrially feasible approach to fabricate different geometries and structures for organic TE modules. So, this approach could provide a good reference for the production of high efficiency, low-temperature, lightweight, low-cost, TE materials.

1. Introduction

In recent decades, thermoelectric (TE) materials have been found to be promising candidates for renewable and green energy applications [1]. These materials are heat engines which convert a temperature difference directly into electrical energy, without requiring any moving parts. This effect can be used to obtain energy from the waste-heat in different sources such as factories and automobiles [2]. Conversely, the TE devices can also convert electrical energy into thermal energy for cooling or heating through the Peltier effect [3]. However, the low efficiency of current TE devices has limited its commercial applications. Therefore, the development of high-performance TE materials becomes a necessary approach for waste-heat recovery. The performance of TE materials are usually evaluated by a dimensionless figure of merit ZT,

$$ZT = \frac{S^2 \sigma}{k} T \tag{1}$$

where σ is the electrical conductivity (S cm^{-1}), S is the Seebeck coefficient (VK^{-1}), T is the absolute temperature (K) and k is the thermal conductivity (Wm^{-1}K^{-1}). The power factor (σS^2) is proportional to the output power of

the TE device. Therefore, the ZT value can be enhanced by increasing the power factor, and/or decreasing the thermal conductivity of the materials.

The most commonly used TE materials are based on inorganic materials, such as Bi_2Te_3 (at near room temperature) [4], PbTe (at medium temperature) [5], and SiGe (at high temperature) [6]. They have high ZT values, however, they suffer from some drawbacks like paucity, toxicity, expensiveness, and complexities in processing [7]. The organic materials have numerous applications in a variety of domains, including transistors, supercapacitors, biosensors, actuators, and optoelectronic devices. Recently, they have attracted widespread research attention for TE applications. Even though they can easily decompose at high temperatures, it should be emphasized that most waste-heat energies are at temperatures below 150 °C [2]. These materials are considered to be promising candidates for a new generation of near-room-temperature TE materials, due to unique advantages such as light weight, low thermal conductivity, chemical stability, high flexibility, and easy preparation. Furthermore, the organic materials are usually soluble in a variety of organic solvents, which make them suitable for roll to roll mass production [8].

Unlike inorganic materials, the thermal conductivity of most organic materials is nearly independent of electrical conductivity and it is in the range of $0.1-0.5\,Wm^{-1}K^{-1}$. This behavior is because of the stronger charge-lattice coupling which leads to poor phonon transport [9]. Furthermore, the phononic contribution to thermal conduction is marginally large compared with the electron part, due to the high electrical resistivity of most polymers [9, 10]. Therefore, thermal conductivity in polymers does not significantly change with the electrical conductivity. So, the power factor would be a good approximation to evaluate the TE performance of organic materials. Up until now, most research has been focused on conducting polymers, including P3HT [11], PEDOT [10] and PANI [12]. However, in comparison with non-conducting polymers, they have some drawbacks such as relatively high cost, poor processability, and low stability, which have hindered their widespread application [13].

Another drawback, in addition to the aforementioned, is that when increasing the thickness of the conducting polymer, aggregates and amorphous regions begin to form that might negatively affect the electrical properties. This is particularly troublesome given that, from a practical standpoint, in order to achieve higher levels of output power, the TE module must be thicker or bulkier. Even though there are some reports of thick film conducting polymers being used for TE applications, it is still challenging to develop a thick or bulky high-performance TE organic material [14, 15]. In contrast, the non-conducting polymers are usually more stable, easily processable, economical, and thermally insulating. However, due to their low electrical conductivity, they are not suitable for TE applications. The enhancement of electrical conductivity of non-conducting polymers by the addition of fillers has been widely documented. The incorporation of fillers into insulator materials forms a connecting path within the polymer matrices which facilitates electron transfer and promotes electrical conductivity [16]. In addition, it is possible to develop 2D and 3D conductive matrix consisting of suitable fillers for the TE applications. Unlike the electrical conductivity, the thermal conductivity of the composites usually remains nearly constant relative to the polymer without fillers. It is due to the interfacial thermal resistance [16–18]. The correlation between the thermal conductivity and the filler content has been widely discussed either theoretically or experimentally. They have confirmed that unlike electrical conductivity, thermal conductivity does not significantly change with filler contents [16, 19–21]. These properties show the potential of filler/insulator polymers as TE materials. However, there are only a few studies on using non-conducting polymers as TE materials, like PDMS/carbon nanotube nanocomposites [22] PVDF/MWCNT nanocomposites [19] and Cellulose-carbon nanotube composite [23].

Cellulose, the most abundant natural polymer, is mainly used to produce paperboard and paper. Cellulose resources are readily sustainable, accessible, and renewable. It is low cost, low density, stable, available, biocompatible, and safe. Its properties can be matched with a variety of applications and for the creation of new materials. Cellulose and its derivatives are used widely in the fiber, food packaging, plastic, pharmaceutical, textile, membrane, and cosmetic industries [24, 25]. Ethyl cellulose (EC) is a linear polysaccharide, which has been derived from cellulose. It has a similar structure with cellulose in which some of the cellulose's hydroxyl groups are substituted with ethyl groups [26]. It is soluble in a variety of organic solvents like ethanol, methanol, toluene, chloroform, and ethyl acetate, which make it suitable for various desired applications. EC is a suitable binder for preparing the printing pastes of different materials like Titania, Silica, and carbon [27, 28]. Thus, EC could be used as a matrix material for conductor-insulator composites, which makes it applicable for printable TE materials. Additionally, it has low thermal conductivity ($0.2\,Wm^{-1}K^{-1}$) [29]. However, to the best of our knowledge, there are no reports about the TE applications of EC.

Graphene, which represents 2D carbon material, has attracted great research interest in the past decade due to its extraordinary properties, including high electrical conductivity, transparency, chemical, and thermal stability, large specific surface area ($2630\,m^2\,g^{-1}$), high electron mobility at room temperatures, and excellent mechanical stability [30–32].

In particular, the nanocomposite materials made of graphene with polymers represent a new class of multifunctional materials having a combination of unique properties of each component enhanced with a synergistic effect [33]. Among them, the combination of graphene with a non-conducting polymer for the formation of conductive polymer composites has been widely investigated for numerous applications in many technological fields such as supercapacitors [34], sensors [35], piezoelectric devices [36, 37], anti-corrosive coatings [38], and electromagnetic interference shielding [39]. As a TE material, pure graphene has a low Seebeck coefficient, however, the polymer composites with Graphene fillers have demonstrated high thermoelectric performance in numerous studies [40, 41].

Here, graphene nanoplatelets (GNPs) were used as fillers to enhance the electrical conductivity of EC. GNPs are an ideal candidate for conductive composites due to their excellent electrical properties, high specific surface areas, and high thermal and chemical stability. GNPs pastes were prepared by using GNPs as fillers and EC as a binder. Then the films were deposited on a glass slide via a blade coating machine. In order to optimize the TE properties, several pastes with different GNPs content were prepared. The weight ratio of GNPs and EC (W_{GNPs}/W_{EC}) ranging from 0.2 to 0.7, were investigated. The electrical conductivity has increased as the amount of filler content has increased. The trend of electrical conductivity as a function of W_{GNPs}/W_{EC} represents percolation behavior. However, the Seebeck coefficients of all of the samples were in the range of 15 to 20 μVK^{-1}. The maximum TE power factor ($\sim 254.0\,nWm^{-1}\,K^{-2}$) was obtained for the ratio of 0.7 at a temperature of 332 K. The pellet was also fabricated from the highest conductive paste, which resulted in the output power of 16.1 nW and 40.3 nW, at a temperature difference of 20 K and 30 K, respectively. Finally, these results show the applicability of EC for making conductive pellets and thick films for TE applications. Additionally, this study emphasizes the use of EC as a green, renewable, and sustainable emerging material in energy applications.
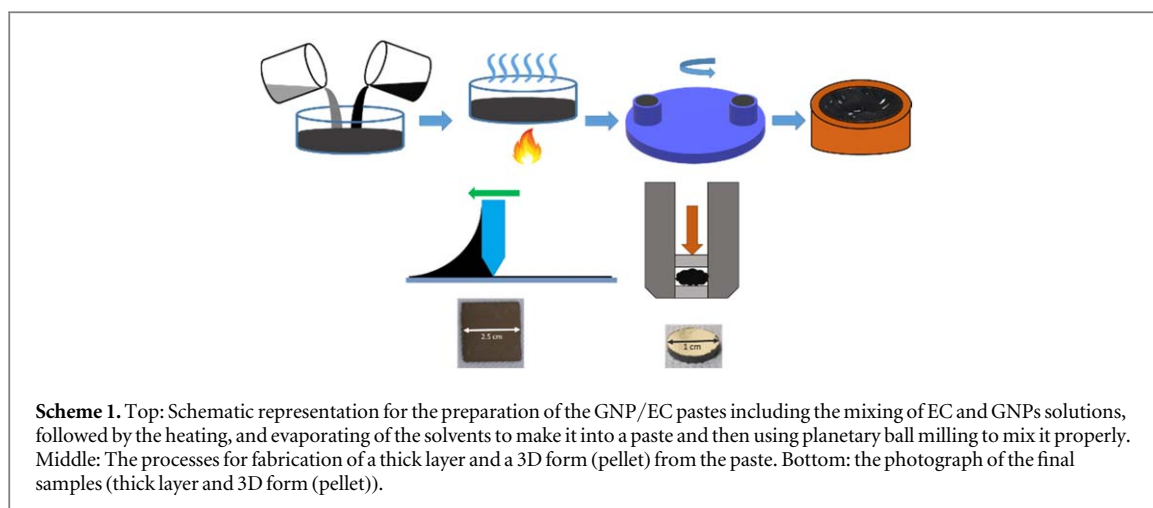
2. Materials and methods

2.1. Materials
Graphene nanoplatelets (GNPs), Ethyl cellulose (EC, 48.0%–49.5% (w/w) ethoxyl basis), de-ionized water, acetic acid, terpineol, ethanol were all purchased and used as received by Sigma Aldrich.

2.2. Preparation of GNPs/EC nanocomposites
GNPs pastes were prepared as follows: 1 gr of GNP powder was dispersed in a mixture of 30 ml of ethanol, 1 ml of acetic acid, and 5 ml of deionized water. Then 27 gr of terpineol was added to the mixture, followed by stirring for one hour. A 10 wt% solution of EC in ethanol was prepared separately and added to the prepared dispersion. Finally, the two prepared solutions were completely mixed by using an ultrasonicator for 30 min and then heated at 60 °C to remove the residual solvents. In the next step, in order to reduce the agglomeration of GNPs and enhance the homogeneity of the mixture, we ground it at 500 rpm for two hours with Pulverisette 7 planetary ball mills (Fritsch, Idar-Oberstein, Germany). The same procedure was repeated with higher amounts of GNPs in order to make pastes with higher GNPs contents. Six pastes with W_{GNPs}/W_{EC} of 0.2, 0.3, 0.4, 0.5, 0.6 and 0.7 were prepared. The films were deposited by blade coating on glass substrates. Then, they were annealed at 120 °C for 45 min which was followed by pressing them at a pressure of 2 Bar for one minute. The silver ink electrodes were deposited on the surface using a shadow mask. The length, width, and distance between the electrodes were 16 mm, 1 mm, and 6 mm, respectively. The thickness of all samples was measured with a profilometer (DektakVeeco 150) in different spots, and then the average value was reported as the thickness. The thicknesses of different samples were in the range of 8 to 12 μm. To prepare the pellets, the similar pastes gradually dropped into the stainless-steel pellet maker at 120 °C to form the pellets. The prepared pellets were annealed again to evaporate all the solvents. Then, the pellets were pressed at room temperature for a period of 1 min with a hydraulic press at a pressure of 5 tons. The height and cross-sectional area of the final device were 1.0 mm, and 0.78 cm^2, respectively.

2.3. Samples characterization
The TE properties were measured using a home-made setup in which two Peltier cells were used to generate the thermal gradient along the device. The thermal probes (Pt100 thermistors) were used to monitor the temperature on the sample. A thermally conductive paste was used to facilitate heat exchange between the Peltier cells and the sample. A Keithley 2420 source meter was used to measure current-voltage (I-V) and open-circuit voltage (V_{OC}) characteristics. The Seebeck coefficients were calculated through the normalizing the potential difference of the device with the temperature difference ($V_{OC}/\Delta T$) when it was set to 5K.

Scheme 1. Top: Schematic representation for the preparation of the GNP/EC pastes including the mixing of EC and GNPs solutions, followed by the heating, and evaporating of the solvents to make it into a paste and then using planetary ball milling to mix it properly. Middle: The processes for fabrication of a thick layer and a 3D form (pellet) from the paste. Bottom: the photograph of the final samples (thick layer and 3D form (pellet)).

The electrical conductivity was calculated with the following equation (2),

$$\sigma = \frac{l}{R\,d\,t} \qquad (2)$$

where R, l, d, and t are the resistance, the distance between the two silver electrodes, the width of the silver electrode, and the thickness of the sample, respectively. To obtain the temperature-dependent resistance, the I-V measurements were performed at different temperatures and the resistance (R) was calculated from the inverse slope of a linear fit of the I-V graph. Finally, the power output of the TE devices was extracted from I-V measurements at different temperature differences.

The sample morphology was investigated with a field-emission scanning electron microscope (FE-SEM), equipped with a Sigma 500 Gemini field emission gun operating at 10 kV. For the SEM characterizations, the original films without any coating were used. The connection between the sample holder and the film was accomplished by copper tape.

3. Results and discussion

Scheme 1 illustrates the schematic representation of the preparation process. As mentioned in the experimental section, it includes three steps, first preparing the pastes, then grinding and blending in the planetary ball milling machine, and finally the deposition of pastes as layers or dropping it to form pellets. The images of the final fabricated samples in both layer and pellet form are shown at the bottom of Scheme 1. Figure 1 compares the low and high-resolution scanning electron microscopy (SEM) images of the EC/GNP layers at different values of W_{GNPs}/W_{EC}. According to the SEM images, the distribution of the GNPs is uniform and homogenous in the samples. The morphologies do not exhibit a clear trend when the ratio increased. In the samples with a low-filler content (EC/GNP 0.2 and EC/GNP 0.3), the SEM images are blurry and only the GNPs' edges are visible. This is to be expected as the SEM creates an image using scattered electrons from the surface and the charges could not scatter from the insulator regions. This leads to a reduction in SEM images quality at the EC/GNP 0.2 and EC/GNP 0.3 samples, since they emit fewer scattered electrons from their surfaces. In other samples (EC/GNPs 0.4, EC/GNPs 0.5, EC/GNPs 0.6, and EC/GNPs 0.7), which have the higher GNPs contents, the GNPs flakes are more distinguishable.

These results highlight that at lower ratios (0.2 and 0.3) the fillers are not connected very well, then by increasing the filler content, the network structure of the GNPs has begun to form. Further increasing the filler content, the composite becomes denser and more connected. The dimension of the flakes is variable between a few hundred nm to more than 20 30μm. The GNPs flakes, as visible in figure 1, are smaller than the average size according to the product specifications, which would have them at 25 micrometers. The difference between this expected size and the current smaller size may be a result of bath sonication and/or grinding by the ball milling machine since GNPs flakes could be broken apart during those processes.

The voltage-current characteristics at room temperature for the GNPs/EC composite samples with different filler contents are shown in figure 2. For all of the samples, the relationship between voltage and current is linear, which illustrates that the ohmic behavior of the nanocomposites within the applied potential window. The room temperature electrical conductivity was calculated based on equation (2). The thicknesses of the samples were reported in table 1. Usually, the electrical conductivity of conductor-insulator composites represents a critical behavior if the filler content reaches the percolation threshold. This behavior typically follows a power-law
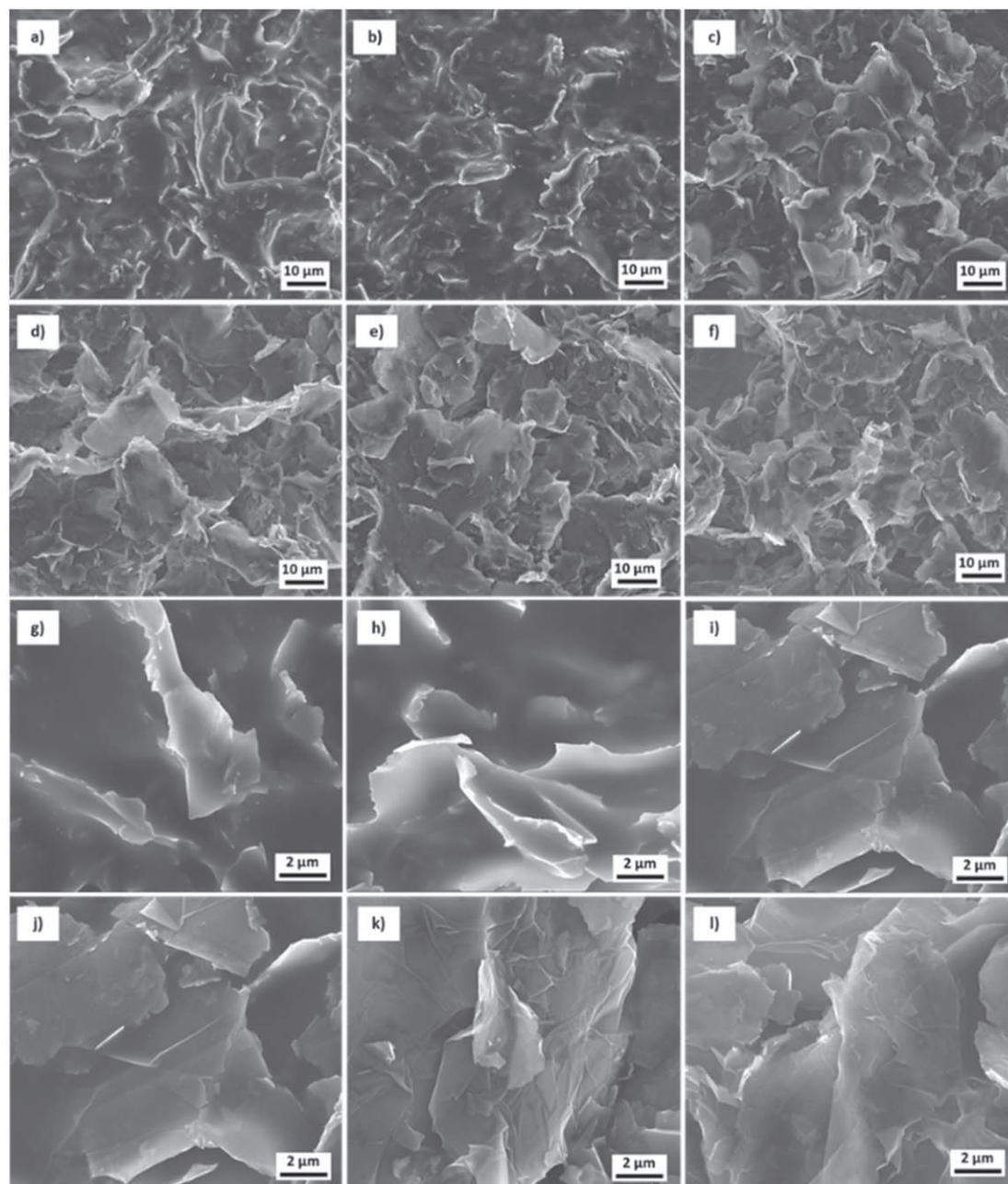
Figure 1. Low- (a)–(f) and high-resolution (g)–(l) FE-SEM images of GNPs/EC composite films with different GNPs contents. GNP/EC 0.2 (a) and (g); GNP/EC 0.3 (b) and (h); GNP/EC 0.4 (c) and (i); GNP/EC 0.5 (d) and (j); GNP/EC 0.6 (e) and (k) and GNP/EC 0.7 (f) and (l).

relationship between filler content and electrical conductivity (equation (3)).

$$\sigma = \sigma_0(\phi - \phi_0)^t \tag{3}$$

where σ (S/m) is the electrical conductivity, σ_0 (S/m) is a constant value determined by a specific material's properties, ϕ (vol%) is the filler content, ϕ_0 (vol%) shows the percolation threshold, and t is the exponent factor which depends on the structure of the composite system. The volume fraction percentage (vol%) of fillers in the different samples were calculated using the densities of EC and GNPs. The densities of EC and GNPs were assumed to be 1.75 g cm^{-3} (according to the specification) and 2.2 g cm^{-3} (a typical reported value for GNPs in the literature like [42]), respectively. As shown in figure 3(a), the plot illustrates the electrical conductivities as a function of vol% of GNPs. At the sample with the lowest filler content (9.4 vol.%), the electrical conductivity is 2.4 Sm^{-1} and it improves by two orders of magnitude (355.4 Sm^{-1}) in the sample with the highest filler content (26.6 vol%). As mentioned, the electrical conductivity of the composite has percolation behavior, followed by equation (2). Considering the experimental data, equation (2) perfectly fits when σ_0, ϕ_0, and t are, 0.00889 $\pm$ 0.00325, 4.63697 $\pm$ 0.49237, and 3.42917 $\pm$ 0.09137, respectively. The coefficient of determination
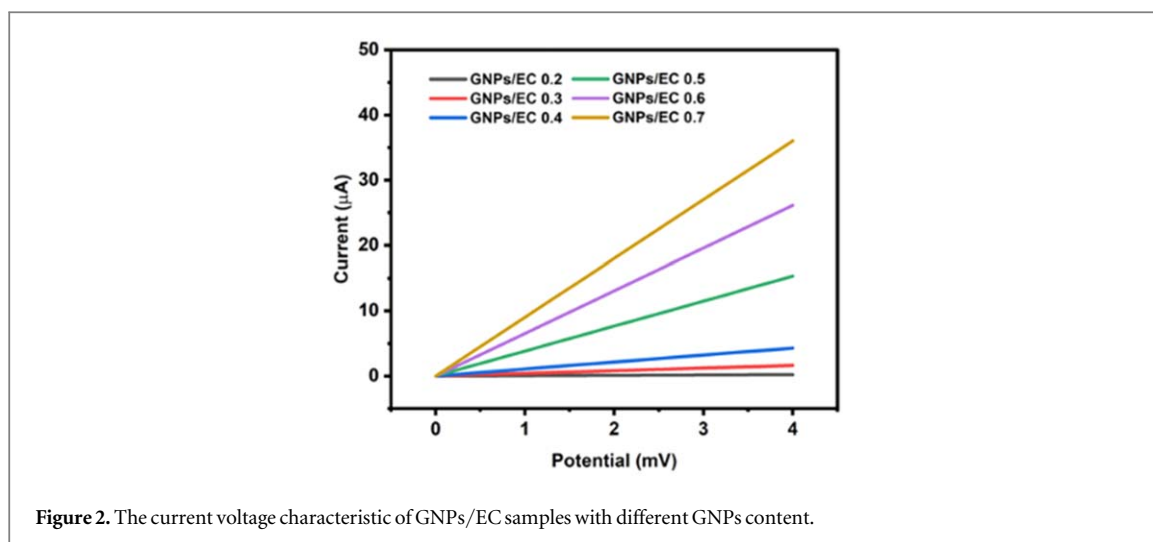
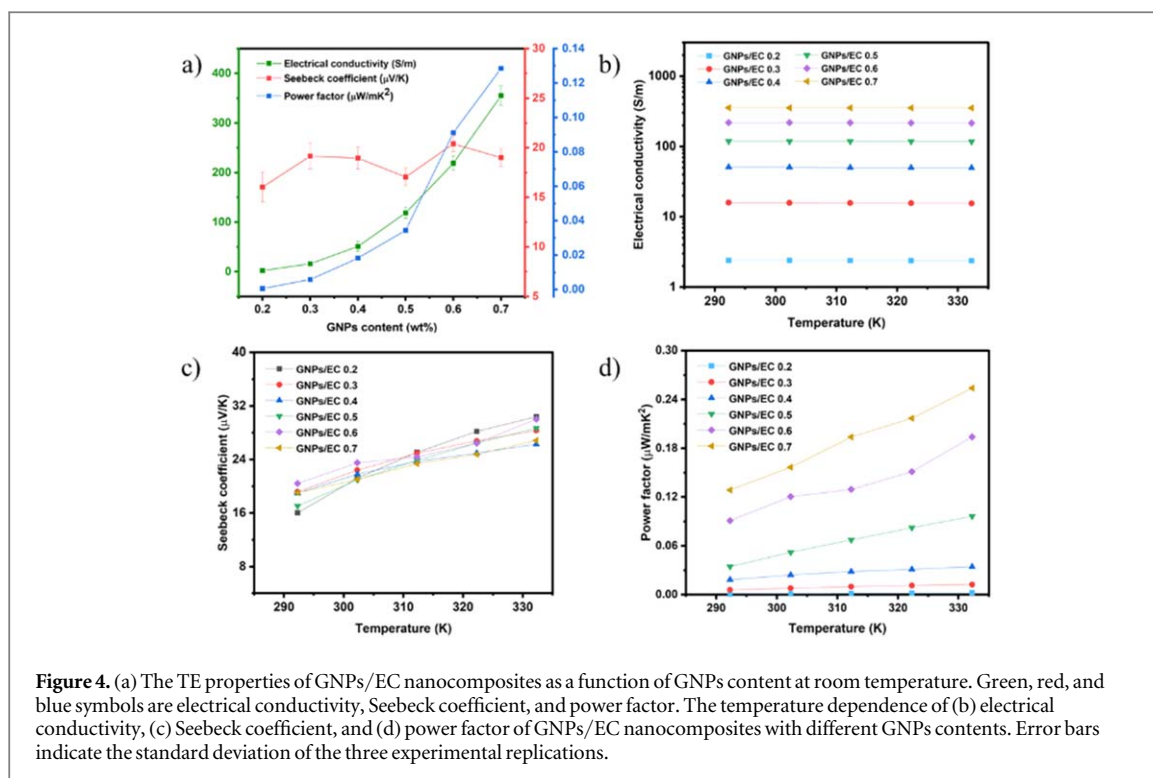**Figure 2.** The current voltage characteristic of GNPs/EC samples with different GNPs content.

Table 1. List of Thicknesses of Different Samples. The error values were calculated from the standard deviation of three repeated measurements.

Sample	GNPs/EC 0.2	GNPs/EC 0.3	GNPs/EC 0.4	GNPs/EC 0.5	GNPs/EC 0.6	GNPs/EC 0.7
Thicknesses (μm)	8.6 ± 0.3	9.6 ± 0.5	10.1 ± 0.4	12.1 ± 0.3	11.2 ± 0.4	9.5 ± 0.5
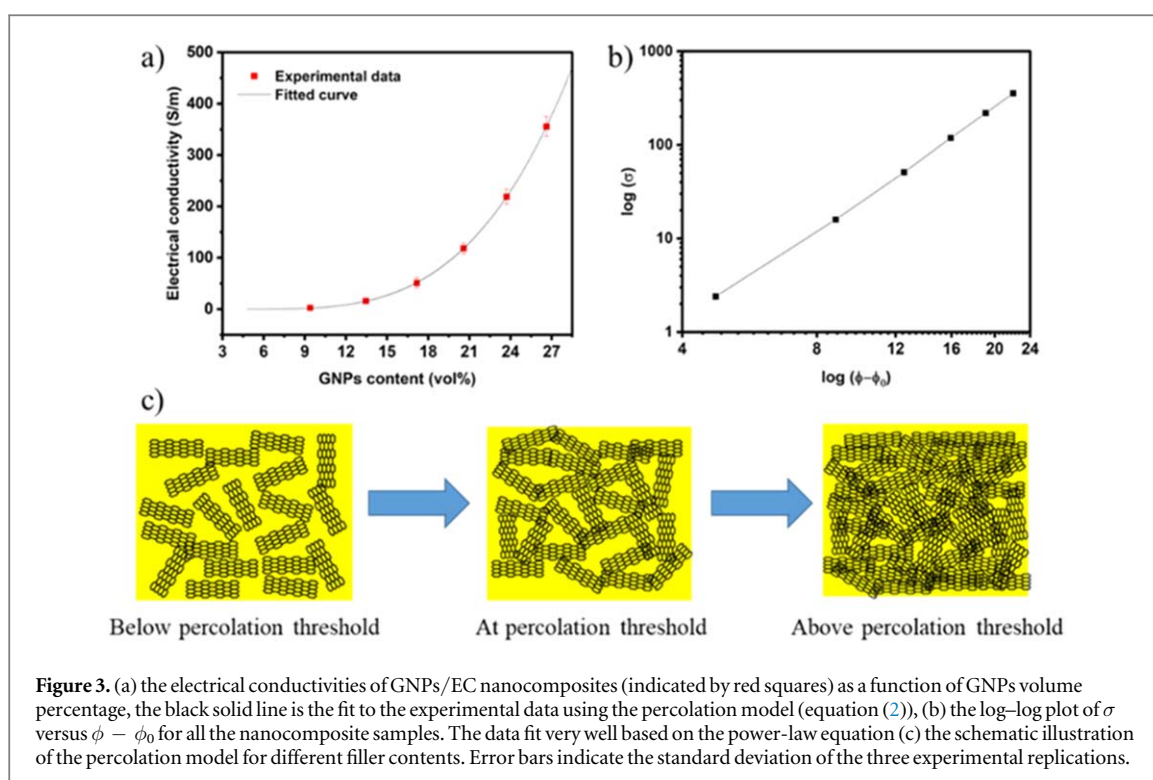
Figure 3. (a) the electrical conductivities of GNPs/EC nanocomposites (indicated by red squares) as a function of GNPs volume percentage, the black solid line is the fit to the experimental data using the percolation model (equation (2)), (b) the log–log plot of σ versus $\phi - \phi_0$ for all the nanocomposite samples. The data fit very well based on the power-law equation (c) the schematic illustration of the percolation model for different filler contents. Error bars indicate the standard deviation of the three experimental replications.

(R^2) is 0.99998 which indicates the data and model's consistency. The plot of $\log(\sigma)$ versus $\log(\phi - \phi_0)$ for the electrical conductivity of all of the samples, as shown in the inset of figure 3(b), shows a linear behavior which indicates the formation of a percolated network of GNPs in the EC matrix with the increase of GNP content. The Schematic representation of the electrical percolation is illustrated in figure 3(c). It shows that, below the percolation threshold, GNPs are separated from each other to form a conductive network, so electron transfers fail to occur and the nanocomposite behaves like an insulator. At the percolation threshold, the electron transport starts up, and adding more fillers leads to an increase in electrical conductivity. This schematic is consistent with SEM characterization which shows that at the samples with a low-filler content, the connection between GNPs flakes is poor. Figure 4(a) summarizes the electrical conductivity, Seebeck coefficient, and power

Figure 4. (a) The TE properties of GNPs/EC nanocomposites as a function of GNPs content at room temperature. Green, red, and blue symbols are electrical conductivity, Seebeck coefficient, and power factor. The temperature dependence of (b) electrical conductivity, (c) Seebeck coefficient, and (d) power factor of GNPs/EC nanocomposites with different GNPs contents. Error bars indicate the standard deviation of the three experimental replications.

factor at room temperature as a function of the filler content. There is not an apparent dependency between filler content and the Seebeck coefficient. This is typical behavior in these kinds of composites [16, 23].

In the filler-insulator polymer, the effective Seebeck coefficient should be a function of fillers' Seebeck. The Seebeck coefficient of pure GNPs was reported less than 11 μV/K at room temperature [19, 43]. The Seebeck coefficients of the nanocomposite films (typically between 15–20 μV/K) are higher than the Seebeck coefficient value of pure GNPs. This phenomenon could be explained by the arrangement of GNPs flakes within the polymer matrix. In the composite films due to the polymer matrices and a large number of filler junctions, the energy filtering effect could scatter the charge carriers with low energy[19, 40]. Hence, the contribution of low-energy charge carriers in the thermovoltage decreases and the Seebeck coefficient would increase. Since the Seebeck coefficient does not change with the filler content, the power factor is mainly dependent on electrical conductivity. The power factor has a similar trend with the electrical conductivity, with a maximum value at the ratio of 0.7. For further investigation of TE properties of composites, the electrical conductivity, Seebeck coefficient, and power factor were measured at higher temperatures. As shown in figure 4(c), for all the samples, the Seebeck coefficient increased along with the increase in temperature. On other hand, there are minor decreases in electrical conductivity (figure 4(b)).

These trends for the Seebeck coefficient and electrical conductivity, when compared to temperature, are a feature of metals. The positive Seebeck coefficient values for all composite samples indicate a p-type TE behavior in which hole carriers play an important role in charge transport. The p-type nature of the nanocomposite could be attributed to the absorption of water and oxygen molecules during exposure to the air [44]. Figure 4(d) shows the temperature-dependent power factor of the different samples. The dependency of power factor and filler content is similar to the electrical conductivity. The maximum TE power factor reaches to 254.0 nWm^{-1}K^{-2} at 332 K for the sample with the highest filler loading. Given that the thermal conductivity does not significantly change with filler loading [16, 19–21], the thermal conductivity of EC (0.2 Wm^{-1} K^{-1} [29]) is a good approximation for the thermal conductivity of the nanocomposite samples. Now, considering the maximum TE power factor, the absolute temperature, and the thermal conductivity of EC, the order of magnitude of ZT can be estimated for the sample with the highest electrical conductivity. According to equation (1), the ZT value is 0.00042. So, the order of magnitude of ZT should be 10^{-4}. To investigate the power generation characteristics of the GNPs/EC nanocomposites, the current-voltage measurements were conducted at a temperature difference of 20 K. Then, the output power was obtained from the multiply of currents and voltages. Figures 5(a) and (b) show the current-voltage and power-voltage characteristics of different composites at a temperature difference of 20 K. The cold and hot sides were kept at temperatures of 292.15K and 312.15 K, respectively. From the theoretical calculation for the maximum value of output power (P$_{max}$) is
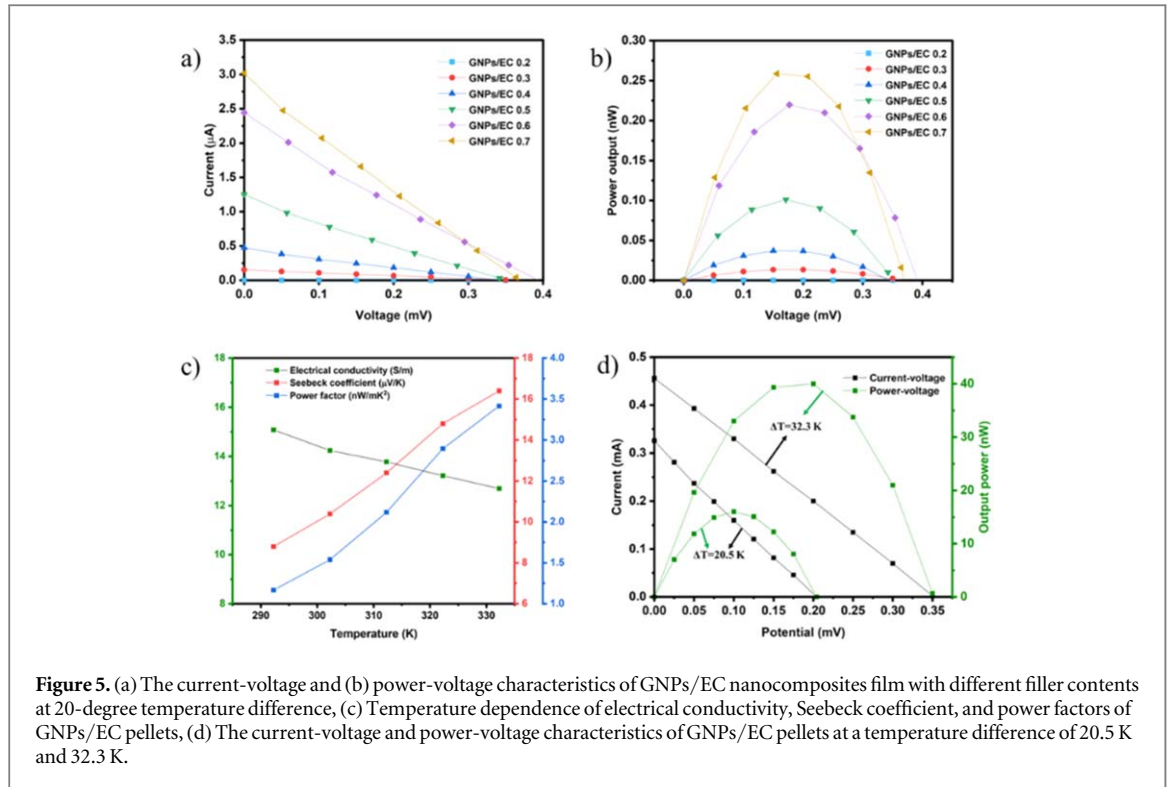
Figure 5. (a) The current-voltage and (b) power-voltage characteristics of GNPs/EC nanocomposites film with different filler contents at 20-degree temperature difference, (c) Temperature dependence of electrical conductivity, Seebeck coefficient, and power factors of GNPs/EC pellets, (d) The current-voltage and power-voltage characteristics of GNPs/EC pellets at a temperature difference of 20.5 K and 32.3 K.

$$P_{max} = \frac{V_{oc}^2}{4R_{In}} \tag{4}$$

where R_{In} and V_{OC} are the internal resistance and the open-circuit voltage, respectively [14]. Hence, the P_{max} of the nanocomposites is proportional to the electrical conductivity, since the variation of the Seebeck coefficient is negligible compared to the electrical conductivity. So, the highest conductive sample results in the highest P_{max} value. The P_{max} of the ratio of 0.2, 0.3, 0.4, 0.5, 0.6 and 0.7 at temperature difference of 20 K were 0.2, 13.4, 37.0, 101.1, 219.8 and 258.7 pW, respectively. Finally, to demonstrate the feasibility of this approach for fabricating 3D structural materials, 3D forms of the devices (pellets) from the most highly conductive pastes were prepared. As mentioned in the experimental section, the paste dropped little by little into a pellet maker, and after drying the solvent at 393.15 K, it was cold-pressed. The electrical conductivity was calculated based on equation (2) at room temperature which is 15.1 Sm^{-1}. The electrical conductivity of the pellet is one order of magnitude less than the thick film.

The different values of electrical conductivity in the vertical and lateral directions could be associated with 2D planar geometry graphene sheets. In the nanocomposites, the charge transfer easily occurs along the sheets, however, the charge does not flow as well in the vertical direction as it does in the lateral direction because in order to move in a vertical direction it needs to jump out of its original plane and into another plane. Since the lateral and vertical electrical conductivities are dependent on different kinds of charge transfer, the former along and across GNPs sheets and the latter between the sheets, their values are different. Notably, due the cross-sectional area and height of pellet, its resistance is 0.85 Ω at room temperature which is much smaller than its thick film counterpart (296.1 Ω).

The thermoelectric properties of the pellet are shown in figure 5(c) at different temperatures. Due to the significant reduction of electrical conductivity, the power factor at room temperature is 1.17 $nWm^{-1} K^{-2}$, which is two orders of magnitude less than its thick film counterpart (616.8 $nWm^{-1} K^{-2}$). The current-voltage characteristic and power generation of the pellet at temperature differences of 20.5 K and 32.3 K were shown in figure 5(d). The corresponding maximum output power of these temperature differences are 16.2 nW and 40.1 nW, respectively. Although the electrical conductivity value of a pellet is much smaller than for a thick film of the same material, the output power has increased two orders of magnitude. The last results highlight the importance of the structural engineering of thermoelectric materials and emphasize the value of output power along with thermoelectric properties.

4. Conclusion

There is a contest to increase the ZT value of TE materials, however, beyond the ZT, it is important to find green, low-cost, available, and easily-processable materials. Herein, Ethyl cellulose (EC), a green and biocompatible material, together with Graphene nanopellets (GNPs) have been used as polymer matrices and fillers, respectively. The nanocomposite with different filler contents were printed with a blade-coating machine. The electrical conductivity values of different composites have increased based on the percolation model which shows that GNPs within an EC matrix have created segregated networks. However, the Seebeck coefficient was not dependent on the filler content. From a device performance point of view, the higher filler content leads to a higher TE performance. Additionally, a pellet from the highest conductive paste was fabricated, showing the potential of the process for achieving higher output power. The proposed strategy is a facile, practical, scalable, easily-processable, and effective approach to fabricate different types of TE devices (planar and vertical). Moreover, it is guaranteed to improve the electrical conductivities, and the Seebeck coefficients of nanocomposites. Overall, it emphasizes the applications of non-conducting polymers rather than using conducting polymers with higher costs and lower processability. A promising direction to further improve the TE properties is the investigation of different fillers, like, for example, adding Carbon nanotubes to improve the electrical conduction in the vertical direction. Given the simplicity of our approach, a similar strategy seems appropriate to fabricate high-performance TE modules.

Acknowledgments

ORCID iDs

Saeed Mardi ⓘ https://orcid.org/0000-0002-7625-1629

References

[1] Bell L E 2008 Cooling, heating, generating power, and recovering waste heat with thermoelectric systems *Science* **321** 1457–61
[2] Toshima N 2017 Recent progress of organic and hybrid thermoelectric materials *Synth. Met.* **225** 3–21
[3] Goldsmid H J 1995 *Conversion Efficiency and Figure-of-Merit CRC Handbook of Thermoelectrics* (United States: Boca Raton) https://scholar.google.com/scholar_lookup?title=Conversion%20efficiency%20and%20figure-of-merit&author=H.%20Goldsmid&publication_year=1995
[4] Xiong X, Zhu L, Wang G, Liu D, Zhang Q and Feng W 2020 Microstructure and properties of n-type Bi 2 Te 3-based thermoelectric material fabricated by selective laser sintering *Mater. Res. Express* **7** 066504
[5] Roychowdhury S and Biswas K 2019 Effect of In and Cd co-doping on the thermoelectric properties of Sn1− xPbxTe *Mater. Res. Express* **6** 104010
[6] Taborda J A P, Romero J J, Abad B, Muñoz-Rojo M, Mello A, Briones F and Gonzalez M S M 2016 Low thermal conductivity and improved thermoelectric performance of nanocrystalline silicon germanium films by sputtering *Nanotechnology* **27** 175401
[7] Chen G, Xu W and Zhu D 2017 Recent advances in organic polymer thermoelectric composites *J. Mater. Chem.* C **5** 4350–60
[8] Yao H, Fan Z, Cheng H, Guan X, Wang C, Sun K and Ouyang J 2018 Recent development of thermoelectric polymers and composites *Macromol. Rapid Commun.* **39** 1700727
[9] Zhang Q, Sun Y, Xu W and Zhu D 2014 Organic thermoelectric materials: emerging green energy materials converting heat to electricity directly and efficiently *Adv. Mater.* **26** 6829–51
[10] Bubnova O, Khan Z U, Malti A, Braun S, Fahlman M, Berggren M and Crispin X 2011 Optimization of the thermoelectric figure of merit in the conducting polymer poly (3, 4-ethylenedioxythiophene) *Nat. Mater.* **10** 429–33
[11] Mardi S, Pea M, Notargiacomo A, Yaghoobi Nia N, Di Carlo A and Reale A 2020 The Molecular Weight Dependence of Thermoelectric Properties of Poly (3-Hexylthiophene) *Materials* **13** 1404
[12] Wang Q, Yao Q, Chang J and Chen L 2012 Enhanced thermoelectric properties of CNT/PANI composite nanofibers by highly orienting the arrangement of polymer chains *J. Mater. Chem.* **22** 17612–8
[13] Aghelinejad M and Leung S N 2018 Fabrication of open-cell thermoelectric polymer nanocomposites by template-assisted multi-walled carbon nanotubes coating *Composites Part B: Engineering* **145** 100–7
[14] Hwang S, Potscavage W J Jr, Nakamichi R and Adachi C 2016 Processing and doping of thick polymer active layers for flexible organic thermoelectric modules *Org. Electron.* **31** 31–40
[15] Endrődi B, Samu G F, Fejes D, Németh Z, Horváth E, Pisoni A, Matus P K, Hernádi K, Visy C and Forró L 2015 Challenges and rewards of the electrosynthesis of macroscopic aligned carbon nanotube array/conducting polymer hybrid assemblies *J. Polym. Sci., Part B: Polym. Phys.* **53** 1507–18
[16] Yu C, Kim Y S, Kim D and Grunlan J C 2008 Thermoelectric behavior of segregated-network polymer nanocomposites *Nano Lett.* **8** 4428–32

[17] Cho S, Kikuchi K, Miyazaki T, Takagi K, Kawasaki A and Tsukada T 2010 Multiwalled carbon nanotubes as a contributing reinforcement phase for the improvement of thermal conductivity in copper matrix composites *Scr. Mater.* **63** 375–8

[18] Kocjan A, Schmidt R, Lazar A, Prado-Gonjal J, Kovač J, Logar M, Mompean F J, Garcia-Hernandez M, Ruiz-Hitzky E and Wicklein B 2018 *In situ* generation of 3D graphene-like networks from cellulose nanofibres in sintered ceramics *Nanoscale* **10** 10488–97

[19] Aghelinejad M and Leung S N 2018 Thermoelectric nanocomposite foams using non-conducting polymers with hybrid 1D and 2D nanofillers *Materials* **11** 1757

[20] Tu H and Ye L 2009 Thermal conductive PS/graphite composites *Polym. Adv. Technol.* **20** 21–7

[21] Shen M, Cui Y, He J and Zhang Y 2011 Thermal conductivity model of filled polymer composites *Int. J. Miner. Metall. Mater.* **18** 623

[22] Khosla A and Gray B L 2009 Preparation, characterization and micromolding of multi-walled carbon nanotube polydimethylsiloxane conducting nanocomposite polymer *Mater. Lett.* **63** 1203–6

[23] Gnanaseelan M, Chen Y, Luo J, Krause B, Pionteck J, Pötschke P and Qi H 2018 Cellulose-carbon nanotube composite aerogels as novel thermoelectric materials *Compos. Sci. Technol.* **163** 133–40

[24] Crowley M M, Schroeder B, Fredersdorf A, Obara S, Talarico M, Kucera S and McGinity J W 2004 Physicochemical properties and mechanism of drug release from ethyl cellulose matrix tablets prepared by direct compression and hot-melt extrusion *Int. J. Pharm.* **269** 509–22

[25] McKeen L W 2017 *Film Properties of Plastics and Elastomers* (United States: William Andrew) https://scholar.google.it/scholar?as_sdt=1,5&q=allintitle:+Film+Properties+of+Plastics+and+Elastomers+author:LW+author:McKeen&hl=en

[26] Davidovich-Pinhas M, Barbut S and Marangoni A G 2014 Physical structure and thermal behavior of ethylcellulose *Cellulose* **21** 3243–55

[27] Behrouznejad F, Taghavinia N and Ghazyani N 2018 Monolithic dye sensitized solar cell with metal foil counter electrode *Org. Electron.* **57** 194–200

[28] Behrouznejad F, Tsai C-M, Narra S, Diau E W-G and Taghavinia N 2017 Interfacial Investigation on Printable Carbon-Based Mesoscopic Perovskite Solar Cells with NiO x/C Back Electrode *ACS Applied Materials & Interfaces* **9** 25204–15

[29] Yang Y 2007 *Thermal conductivity Physical Properties of Polymers Handbook* (Berlin: Springer) pp 155–63

[30] Allen M J, Tung V C and Kaner R B 2010 Honeycomb carbon: a review of graphene *Chem. Rev.* **110** 132–45

[31] Geim A K and Novoselov K S 2010 *The Rise of Graphene Nanoscience and Technology: A Collection of Reviews from Nature Journals* (Singapore: World Scientific) pp 11–9

[32] Byranvand M M, Tajabadi F, Mardi S, Taghavinia N, Zarandi A A and Dabirian A 2019 Controlled electrophoretic deposition of electrochemically exfoliated graphene sheets on Ag nanowires network *Micro & Nano Letters* **14** 389–93

[33] Chee W K, Lim H N, Huang N M and Harrison I 2015 Nanocomposites of graphene/polymers: a review *RSC Adv.* **5** 68014–51

[34] Yan J, Wei T, Shao B, Ma F, Fan Z, Zhang M, Zheng C, Shang Y, Qian W and Wei F 2010 Electrochemical properties of graphene nanosheet/carbon black composites as electrodes for supercapacitors *Carbon* **48** 1731–7

[35] Wang S, Xie G, Su Y, Su L, Zhang Q, Du H, Tai H and Jiang Y 2018 Reduced graphene oxide-polyethylene oxide composite films for humidity sensing via quartz crystal microbalance *Sensors Actuators* B **255** 2203–10

[36] Tung T T, Karunagaran R, Tran D N H, Gao B, Nag-Chowdhury S, Pillin I, Castro M, Feller J-F and Losic D 2016 Engineering of graphene/epoxy nanocomposites with improved distribution of graphene nanosheets for advanced piezo-resistive mechanical sensing *J. Mater. Chem.* C **4** 3422–30

[37] Rahman M A and Chung G-S 2013 Synthesis of PVDF-graphene nanocomposites and their properties *J. Alloys Compd.* **581** 724–30

[38] Singh B P, Jena B K, Bhattacharjee S and Besra L 2013 Development of oxidation and corrosion resistance hydrophobic graphene oxide-polymer composite coating on copper *Surf. Coat. Technol.* **232** 475–81

[39] Liang J, Wang Y, Huang Y, Ma Y, Liu Z, Cai J, Zhang C, Gao H and Chen Y 2009 Electromagnetic interference shielding of graphene/epoxy composites *Carbon* **47** 922–5

[40] Abad B, Alda I, Díaz-Chao P, Kawakami H, Almarza A, Amantia D, Gutierrez D, Aubouy L and Martín-González M 2013 Improved power factor of polyaniline nanocomposites with exfoliated graphene nanoplatelets (GNPs) *J. Mater. Chem.* A **1** 10450–7

[41] Dey A, Bajpai O P, Sikder A K, Chattopadhyay S and Khan M A S 2016 Recent advances in CNT/graphene based thermoelectric polymer nanocomposite: A proficient move towards waste energy harvesting *Renew. Sustain. Energy Rev.* **53** 653–71

[42] Rashad M, Pan F, Yu Z, Asif M, Lin H and Pan R 2015 Investigation on microstructural, mechanical and electrochemical properties of aluminum composites reinforced with graphene nanoplatelets *Progress in Natural Science: Materials International* **25** 460–70

[43] Xiang J and Drzal L T 2012 Templated growth of polyaniline on exfoliated graphene nanoplatelets (GNP) and its thermoelectric properties *Polymer* **53** 4202–10

[44] Yeom D-Y, Jeon W, Tu N D K, Yeo S Y, Lee S-S, Sung B J, Chang H, Lim J A and Kim H 2015 High-concentration boron doping of graphene nanoplatelets by simple thermal annealing and their supercapacitive properties *Sci. Rep.* **5** 9817